

# Critical and Near-Critical Branching Processes

Johan Chu and Christoph Adami

*W. K. Kellogg Radiation Laboratory*

*California Institute of Technology, Pasadena, California 91125, USA*

(December 1998)

Scale-free dynamics in physical and biological systems can arise from a variety of causes. Here, we explore a branching process which leads to such dynamics. We find conditions for the appearance of power laws and study quantitatively what happens to these power laws when such conditions are violated. From a branching process model, we predict the behavior of three systems which seem to exhibit near scale-free behavior—rank-frequency distributions of number of subtaxa in biology, abundance distributions of genotypes in an artificial life system, and distributions of avalanche sizes in the Bak-Tang-Wiesenfeld sandpile model.

## I. INTRODUCTION

Scale-free distributions, or *power laws*, have been observed in a variety of biological, chemical and physical systems. Such distributions can arise from different underlying mechanisms, but always involve a *separation* of scales, which forces the distribution to take a standard form. Scale-free distributions are most often observed in the distribution of sizes of events (such as the Gutenberg-Richter law [1]), the distribution of times between events (e.g., the inter-event interval distribution in neuronal spike trains [2]), and frequencies. An example of the latter is the well-known and ubiquitous  $1/f$  noise. Some systems are even more interesting because they seem to exhibit self-organization or self-tuning, concomitant with scale-free behavior as an inherent and robust property of the system, not due to the tuning of a control parameter by the experimenter.

Two systems to which such spontaneous scale-free behavior has been attributed are sandpile models and taxon creation in biological systems. The former has served as the paradigm of “self-organized criticality” (SOC) [3], while the latter, manifested in the form of near power law shapes of rank-abundance curves, has been advanced as evidence of a fractal geometry of evolution [4].

A much simpler system where power laws are observed is the random walk [5]. For example, the waiting times  $t$  for first return to zero of the simple random walk in one dimension (starting at  $x = 0$ , at each time step,  $x(t+1) = x(t) \pm 1$  with equal probability) have a probability distribution  $\sim t^{-3/2}$ . Closely related to random walks, branching processes [6] can also create power law distributions. They have been used to model the dynamics of many systems in a wide variety of disciplines, including demography, genetics, ecology, physiology, chemistry, nuclear physics, and astrophysics. Here, we use a branching process to model the creation and growth of evolutionary taxa, and the propagation of avalanches in SOC sandpile models.

In Section II, we examine the properties of the *Galton-Watson* process. We find that this process can generate power laws by appropriate tuning of a control parameter, and examine the dynamics of the system both at the

critical point and away from it. In Section III, we apply this branching process model to various systems, including the taxonomic rank-frequency abundance patterns of evolution and the avalanche size distribution of sandpile models, and discuss the universality of their underlying dynamics. Finally, in Section IV, we discuss the implications of our work, including a discussion of the order and control parameters for the branching process and its applications, and suggest further questions.

## II. THE BRANCHING PROCESS

The Galton-Watson branching process was first introduced in 1874 to explain the disappearance of family names among the British peerage [7]. It is the first branching process in the literature, and also one of the simplest. Consider an organism which replicates. The number of replicants (*daughters*) it spawns is determined probabilistically, with  $p_i$  ( $i = 0, 1, 2, \dots$ ) being the probability of having  $i$  daughters. Each daughter replicates (with the same  $p_i$  as the original organism) and the daughter’s daughters replicate and so on. We are interested in the rank-frequency probability distribution  $P(n)$  of the total number of organisms descended from this organism plus 1 (for the original organism), i.e., the historical size of the “colony” the ancestral replicant has given rise to. Note that this is equivalent to asking for the probability distribution of the length of a random walk starting from 1 and returning to 0 with step sizes given by  $P(\Delta n) = p_{i-1}$  ( $i = 0, 1, 2, \dots$ ) [8].

The abundance distribution  $P(n)$  can be found by defining a generating function

$$F(s) = \sum_{i=1}^{\infty} P(i)s^i. \quad (1)$$

This function satisfies the relationship

$$F(s) = s \sum_{i=0}^{\infty} p_i [F(s)]^i, \quad (2)$$

from which each  $P(n)$  can be determined by equating coefficients of the same order in  $s$  [6]. This result can also be written as

$$P(n) = \frac{1}{n} Q(n, n-1) \quad (k \geq 1), \quad (3)$$

where  $Q(i, j)$  is defined as the probability that  $j$  organisms will give birth to a total of  $i$  true daughters [5]. However, these approaches are not numerically efficient, as the calculation of  $P(n)$  for each new value of  $n$  requires recalculation of each term in the result.

For our present purposes, we approach the problem in a different manner. Let  $P_{k|j}$  be the probability that given  $j$  original organisms, we end up with a total of  $k$  organisms after all organisms have finished replicating. Obviously,

$$P_{k|j} = 0 \quad (k > j), \quad (4)$$

since it is impossible to have less total organisms than one starts out with, and

$$P_{1|1} = p_0, \quad (5)$$

i.e., the probability for one organism to have no daughters. A little less obviously,

$$P_{k|1} = \sum_{j=1}^{k-1} p_j P_{(k-1)|j}, \quad (6)$$

$$P_{k|j} = \sum_{i=1}^{k-1} P_{i|1} P_{i|(j-1)} \quad (j \geq k > 1). \quad (7)$$

These equations allow us to use dynamic programming techniques to calculate  $P(n)$  ( $= P_{n|1}$ ), significantly reducing the computational time required. Also, from Eq. (6), we can write

$$\frac{P_{n|1}}{P_{(n-1)|1}} = p_1 + p_2 \frac{P_{(n-1)|2}}{P_{(n-1)|1}} + p_3 \frac{P_{(n-1)|3}}{P_{(n-1)|1}} + \dots . \quad (8)$$

Since, for  $n \rightarrow \infty$ ,  $P_{n|j}$  is uniformly decreasing, we see

$$\frac{P(n)}{P(n-1)} = \frac{P_{n|1}}{P_{(n-1)|1}} \rightarrow C \text{ as } n \rightarrow \infty, \quad (C \leq 1) \quad (9)$$

where  $C$  is a constant.  $C$  indicates the asymptotic behavior of  $P(n)$  as  $n \rightarrow \infty$ . If  $C < 1$ , the probability distribution is asymptotically exponential, while for  $C = 1$ , the probability distribution is a power law with exponent  $-3/2$ .

Let us now examine the behavior of  $P(n)$  when  $n \lesssim 10^4$ , the more relevant case in the examples to follow. Using Eqs. (4)-(7), we can numerically calculate  $P(n)$  for different sets of  $p_i$ . We define  $m$  as the expected number of daughters per organism, given a set of probabilities  $p_i$ ;

$$m = \sum_i i \cdot p_i. \quad (10)$$

We see that the branching rate  $m$  (the *control parameter*) is a good indicator of the shape of the probability curve (Fig. 1). When  $m$  is close to 1, the distribution is nearly a power law, and the further  $m$  diverges from 1, the further the curve diverges from a power law towards an exponential. When  $m = 1/2$ , the curve is completely exponential. For a population of organisms,  $m$  is a measure of the tendency for new generations to grow, or shrink, in number. A value of  $m > 1$  indicates a growing generation size, which implies that there will, on average, be no generation with no daughters, and that the expected number of total organisms is infinite. Conversely,  $m < 1$  indicates a shrinking population size: There will be a final generation with no daughters, and the expected number of organisms is finite. When  $m = 1$ , the system is in between the two regimes, and only then is a power law distribution found. In the following section, we explore systems where the “organisms” are individual members of species, taxons in a taxonomic tree, or tumbling sites in a sandpile model, and  $m$  is the average number of exact copies an individual makes of itself, the average number of new taxons of the same supertaxon a taxon spawns, or the average number of new tumbles directly caused by a tumbling site.

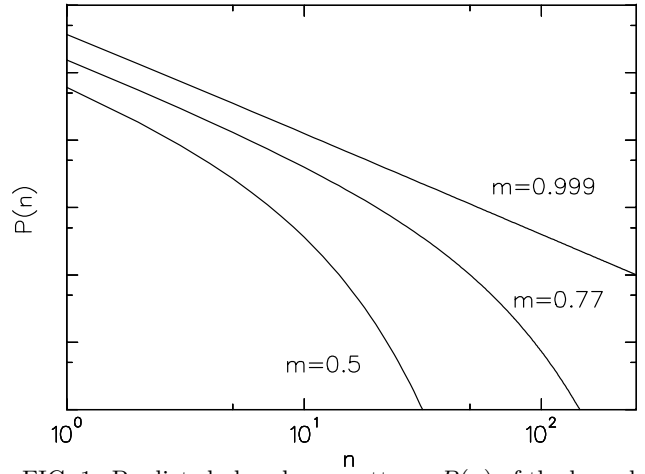


FIG. 1. Predicted abundance patterns  $P(n)$  of the branching model with different values of  $m$ . The curves have been individually rescaled.

### III. APPLICATIONS

#### A. Neutral Model

We first present a simple simulation to test our analysis and lay the groundwork for the exploration of more complicated systems. Consider a population of organisms on a finite two-dimensional Euclidean lattice, one organism to a grid square. Each organism can be *viable* or *sterile*. All viable organisms replicate approximately every  $\tau$  time steps (there is a small random component to each

individual's replication time to avoid synchronization effects), while sterile organisms do not replicate. When an organism replicates, its daughter replaces the oldest organism in the parent's 9-site neighborhood (Fig. 2). We define the *fidelity*  $F$  as the probability that the organism will create a daughter of the same type as itself and the corresponding *genomic mutation rate*  $R$  ( $= 1 - F$ ) at which it creates copies different from itself. The genomic mutation rate is actually the sum of two rates, a probability  $R_n$  for the daughter to be viable but to be of a new *genotype*, different from that of the parent (*neutrality rate*), and a probability  $R_s$  of the daughter being sterile. Of course,  $R_n + R_s = R$ . Note that all viable mutant daughters still share the same replication time  $\tau$ —all mutations are neutral (See Fig. 3). Such a system gives rise to abundance distributions of power law and near-power law type, which can be predicted as follows.

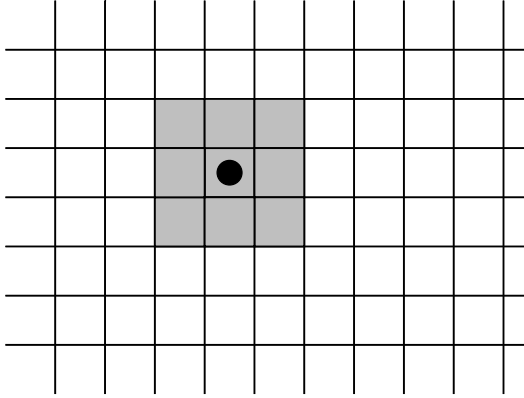


FIG. 2. Neutral model grid. The organisms live on an Euclidean grid, one organism to a site. When an organism replicates, its daughter replaces the oldest organism in the 9-site neighborhood. (If the organism marked by a black dot replicates, its daughter replaces one of the organisms at a gray site.)

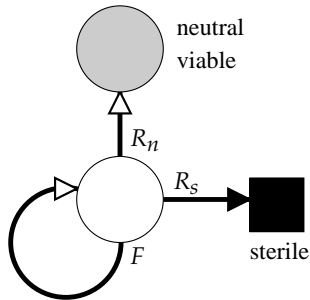


FIG. 3. Neutral replications and mutations. An organism's daughter is of the same genotype as the organism with probability  $F$ , it is of a new, viable genotype with probability  $R_n$ , and it is sterile with probability  $R_s$  such that  $F + R_n + R_s = 1$ .

The total number of organisms is determined by the size of the grid. We write equilibrium conditions for the

total number of organisms  $\rho_A$ , and for the total number of viable organisms  $\rho_V$ ,

$$\Delta\rho_A \sim a\rho_V - \rho_A = 0, \quad (11)$$

$$\Delta\rho_V \sim v\rho_V - \rho_V = 0, \quad (12)$$

where  $a$  is the average number of daughters (viable and sterile) a viable organism has, and  $v$  is the average number of viable daughters a viable organism has. Introducing  $m$ —the average number of true daughters (daughters which share the parent's genotype) for a viable organism—we see that

$$v = \frac{F + R_n}{F}m = (F + R_n)a. \quad (13)$$

From Eqs. (11)-(13), we obtain steady state solutions for  $a$  and  $m$ ,

$$a = \frac{F^{-1}}{1 + \frac{R_n}{F}}, \quad (14)$$

$$m = \frac{1}{1 + \frac{R_n}{F}}. \quad (15)$$

Using the branching process model, we can predict the abundance curve from the values of  $a$  and  $m$  (or conversely,  $F$  and  $R_n$ ). Fig. 4 shows abundance data for two neutral model runs with differing values of  $R_n$  (and consequently  $m$ ), along with predicted distributions (which use only  $R_n$  and  $F$  as parameters) based on the branching model. Although the distribution patterns are very different, both are fit extremely well by the branching process model's predicted curves. In Eq. (15), note that  $R_n$  is the rate of influx of new genotypes (and therefore new competitors for space), while  $F$  is the rate of growth of existing genotypes. The value of  $m$  is determined by the ratio of these two rates. Unless the total number of creatures is increasing,  $m \leq 1$  ( $m = 1$  if and only if  $R_n \rightarrow 0$  and new competing genotypes are introduced at a vanishing rate).

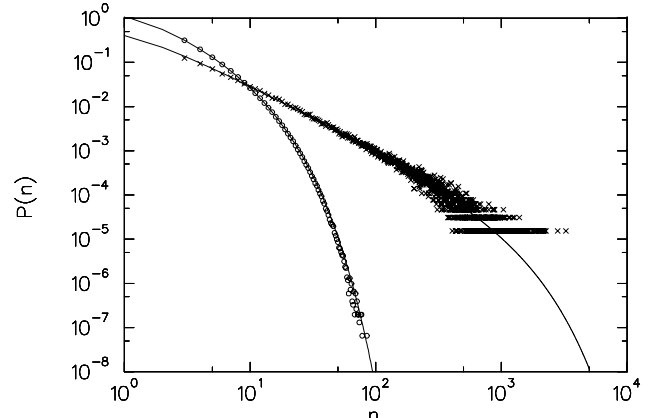


FIG. 4. Abundance distributions and predicted curves for two neutral model runs. The run shown by circles ( $\sim 1.5$  million data points) had a grid size of  $3000 \times 3000$ ,  $F = 0.5$ , and  $R_n = 0.5$ , while the one represented by crosses ( $\sim 0.6$  million data points) had a grid size of  $100 \times 100$ ,  $F = 0.2$ , and  $R_n = 0.1$ .

## B. Artificial Life

Our next system is the artificial life system **sanda** [9], an example of environments which host digital organisms [10]. In this system, while the organisms occupy a two-dimensional grid as in the neutral model detailed above, the organisms are no longer simple, and instead each has a complex genotype consisting of a string of assembly language-like instructions (Fig. 5). Each organism independently executes the instructions of its genotype, and this genotype determines the organism's replication time  $\tau$ . Unlike the neutral model, the system allows non-neutral mutations which lead to new genotypes with both lower and higher replication times than the parent.

The system and the instructions are designed so that the organisms can self-replicate by executing certain sequences of instructions. The replication time of an organism is not a predetermined constant, rather it is determined by the genotype of the organism: Organisms can replicate faster or slower than other competing organisms with different genotypes. For an organism to successfully replicate, its genotype must contain information which allows the organism to allocate temporary space (memory) for its daughter, replicate its genotype (one instruction at a time) into this temporary space, and then to divide, placing its daughter in a grid site of its own (Fig. 5). As in the neutral model, on division, the daughter replaces the oldest organism in its parent's 9-site neighborhood.

Organisms, depending on their genotype, may not be able to replicate (may be sterile) or may only be able to replicate imperfectly (resulting in no true daughters). Also, the **copy** instruction, which the organisms must use to copy instructions from their own code into that of their nascent daughters, has a probability of failure (*copy mutation rate*), which can be set by the experimenter. When the **copy** instruction fails, an instruction is randomly chosen from all the instructions available to the organisms (the *instruction set*) and written in the string location copied to. Copy mutations also lead to non-true daughters. The instruction set is robust; copy errors (mutations) induced during the replication of viable organisms have a non-vanishing probability of creating viable new organisms and genotypes. Indeed, by selecting for certain traits (such as the ability to perform binary logical operations) by increasing the relative speed at which instructions are executed in organisms which carry these traits, the system can be forced to *evolve* and find novel genotypes which contain more information (and less entropy) than their ancestors. Even without this external selection, the system evolves organisms (and genotypes) which replicate more efficiently in less executed instructions.

As a result of this evolution, the fidelity and neutral mutation rate are not fixed, but can vary with the length of an organism's genome and the instructions contained

therein. Also, new genotypes formed by beneficial mutations that allow faster replication than previously existing genotypes will have (on average) an increasing number of organisms— $m > 1$ —until the new, faster replicating genotypes fill up a sizable portion of the grid. All these factors combine to make predicting the abundance distributions for **sanda** much harder than for the neutral model.

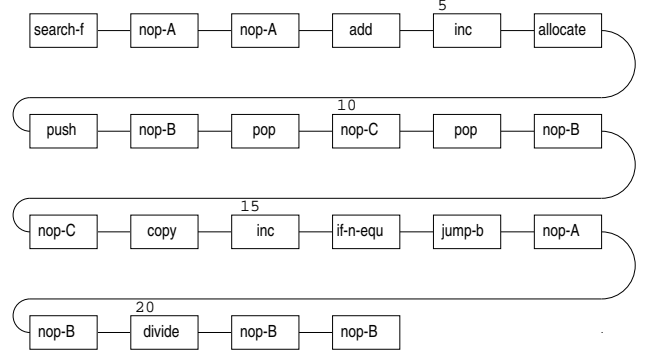


FIG. 5. Example **sanda** genotype. Sanda organisms have genotypes which are strings of **sanda** code. The string shown above replicates by: searching forward (instruction 1) for the complement of the template **nop-A** **nop-A** (2-3), which is **nop-B** **nop-B** (21-22), manipulating this value in an internal register to find the genotype length (4-5), allocating enough memory to store code of genotype length (6), setting registers to prepare for copying (7-11), copying the instructions one at a time (12-19) until all instructions have been copied (15-16), and replicating (20)—placing the daughter in its own grid site. Execution restarts at the beginning of the genotype when the end of the genotype is reached, and continues until the organism is replaced by the newly replicated daughter of another organism (or its own daughter). The **copy** command (14 in this particular genotype) fails and writes a random instruction with probability  $\gamma$ .

Indeed, rather than being constant during the course of a **sanda** experiment,  $R_n$  and  $F$  will vary unpredictably as the population of organisms occupies different areas in genotypic phase space. Certain genotypes may be *brittle*, allowing very few mutations that result in new viable genotypes. The length of the organisms may change, changing both the genomic mutation rate and the neutrality rate. Genotypes exist which make systematic errors when copying, which decreases the fidelity. In short, the dynamics of these digital organisms are complex and messy, much like those of their biochemical brethren. These variations are observed at the same time across different organisms in the population, and are also observed with the progression of time. Still, we attempt to predict the abundance distributions by approximating the ratio of neutral mutations to true copies by the *observed* ratio of viable genotypes to total number of viable organisms ever created:

$$\frac{R_n}{F} \simeq \frac{N_g}{N_v}, \quad (16)$$

where  $N_g$  is the total number of viable genotypes observed during a **sanda** run and  $N_v$  is the total number of viable organisms. This relation should hold approximately under equilibrium conditions. Then, Eq. (15) becomes

$$m \simeq \left(1 + \frac{N_g}{N_v}\right)^{-1}, \quad (17)$$

and from Eq. (14)

$$a = \frac{m}{F}. \quad (18)$$

The fidelity  $F$  is inferred from the average length  $l$  of genotypes during a run and the (externally enforced) per-instruction copy mutation rate  $\gamma$ ,  $F = (1 - \gamma)^l$ . Because we estimate  $m$  and  $a$  from macroscopic observables averaged over the length of a run, we expect some error in our results due to the shifting dynamics of the evolution of genotypes as the system moves in genotypic phase space.

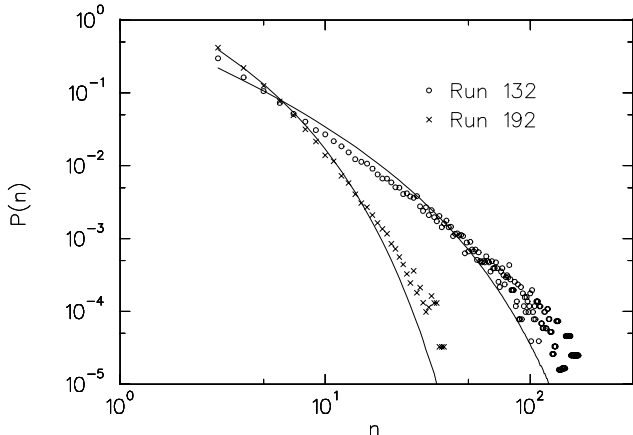


FIG. 6. Abundance data from two **sanda** runs with predicted abundance curves. Both runs were started with the same initial genotype for all organisms, the same per-instruction copy mutation rate ( $\gamma$ ), and the same grid size ( $100 \times 100$ ). Run 192's genotypes evolved into a regime of genotypic phase space with longer average length, and therefore lower fidelity  $F$  and higher neutrality  $R_n$ , than Run 132, resulting in the differences in the abundance distributions. The predicted curves were generated by approximating a representative value of  $R_n/F$  from the ratio of the number of viable genotypes to the number of viable organisms observed over the run. The data was binned using the template threshold method with  $T = 1$  (see Appendix).

The abundance data from two different **sanda** runs are shown in Fig. 6 with the predicted abundance curves. The two runs shared the same grid size and per-instruction copy mutation rate, and were started with the same initial genotypes, but the runs evolved into different regions of genotypic phase space and consequently had significantly different statistics. Considering the many gross approximations we have made, the agreement between our prediction and the experimental data is surprisingly good (especially as no fitting is involved). **Sanda**

is most closely related to an asexually replicating biological population, such as colonies of certain types of bacteria occupying a single niche. The genotype abundance distributions measured in **sanda** are analogous to the species or subspecies abundance distributions of its biological counterparts. In general, species abundance distributions are complicated by the effects of sexual reproduction, and of the localized and variable influences of other species and the environment on species abundances. However, we believe the branching model—used judiciously—can be helpful in the study of such distributions as well.

### C. Evolution

Rank-abundance distributions at taxonomic levels higher than species (e.g., the distribution of the number of families per order) are simpler to model than species abundance distributions, as the effects of the complications noted above are weak or nonexistent. We find that the available data is well fit by assuming no direct interaction or fitness difference between taxa [11]. The shapes of rank-frequency distributions of taxonomic and evolutionary assemblages found in nature are surprisingly uniform. Indeed, Burlando has speculated that all higher-order taxonomic rank-frequency distributions follow power laws stemming from underlying fractal dynamics [4]. We believe this conclusion is hasty: The divergence of the distributions from power law can be observed by applying appropriate binning methods to the data. (See Appendix.) Yule [12] attempted a branching process model explanation of these distributions, and claimed that divergence from power law of rank-abundance patterns was transient and indicated a finite time since the creation of the evolutionary assemblage. Our model indicates that this is not generally the case. We find that the divergence from power law is not a result of disequilibration, but is an inherent property of the evolutionary assemblage under consideration and that this divergence provides insight into microscopic properties of the assemblage (e.g., the rate of innovation).

Say, for example, that we are interested in the rank-frequency distribution of the number of families in each order for fossil marine animal orders. We assume that all new families and orders in this assemblage originate from mutations in extant families. Then, we can define rates of successful mutation  $R_f$  for mutations which create new families in the same order as the original family, and  $R_o$  for mutations which create an entirely new order. In this case, unlike the cases treated above, we approximate  $a \rightarrow \infty$ ; many individual births and mutations occur, but the proportion that are family- or order-forming is minuscule. Finally, assuming a quasi-steady state (the total numbers of orders and families vary slowly [13]), we rewrite Eq. (15),

$$m \simeq (1 + \frac{R_o}{R_f})^{-1} \quad (19)$$

$$\simeq (1 + \frac{N_o}{N_f})^{-1}, \quad (20)$$

in terms of  $N_o$  and  $N_f$ , the total numbers of orders and families respectively. As in the previous systems studied,  $R_o$  is the rate of creation of new—competing—orders, while  $R_f$  is the rate of growth of existing orders, and  $m$  is determined by their ratio.

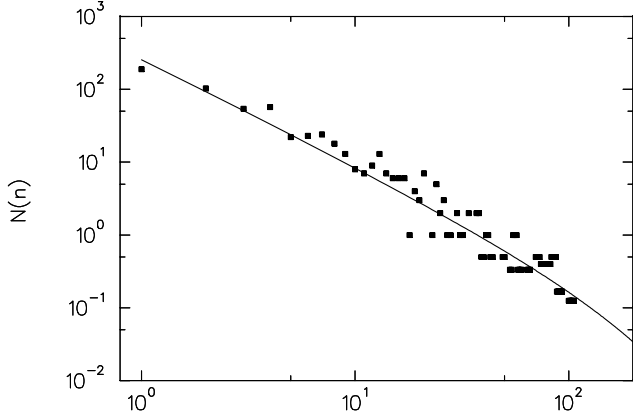


FIG. 7. The rank-frequency distribution of fossil marine animal orders (squares) [14] and the predicted abundance curve (line). The predicted curve was generated—with no free parameters—by approximating  $R_o/F$  by  $N_o/N_f = 0.115$ . The empirical distribution agrees with the predicted curve with significance 0.12 using the Kolmogorov-Smirnov test [11]. The fossil data is shown binned using the template threshold binning method explained in the Appendix with  $T = 1$ .

Data for the abundance distribution of number of families in fossil marine animal orders [14] are shown in Fig. 7. We obtained values for  $N_o$  and  $N_f$  directly from the fossil data to generate the predicted curve with *no free parameters*. The agreement is very good, much better than that for the **sanda** runs where evolutionary parameters such as the fidelity  $F$  and the neutrality  $R_n$  were constantly changing. Comparing  $m$  and the resultant abundance curves with those obtained above for the rank-abundance distribution of **sanda** genotypes leads us to the expected conclusion that the probability of creation of a new genotype in **sanda** per birth is much higher than the probability of a new family creating an order in natural evolution. Indeed, a wide variety of higher-order taxonomic assemblages have abundance distributions consistent with  $m$  near 1 [4]. We believe this is a robust result of the evolutionary process. Low values of  $m$  may not be observed for large taxon assemblages for several reasons. A small value of  $m$  implies either a small number of individuals in the assemblage, or a very specialized niche with a very low rate of taxon formation. A low number of individuals would lead to a low probability of the taxon being discovered and catalogued by biologists. A small number of individuals and taxons would result in an assemblage

with too few taxons to give us a clear statistical picture. Also, since such an assemblage would have a small population, be incapable of further adaptation, or both, we expect it would be more susceptible to competition and environmental effects leading to early extinction.

#### D. Sandpile Models

The Bak, Tang, and Wiesenfeld (BTW) sandpile model [3] is defined on a  $d$ -dimensional lattice. Each site on the lattice has an *energy*  $z_i$  associated with it. A “grain” of energy of size 1 is dropped on a random site  $i$  and if the resultant energy of that site is greater than a critical energy ( $z_i > z_c = 2d - 1$ ), the site transfers energy to its neighbors;

$$z_i \rightarrow z_i - z_c, \quad (21)$$

$$z_n \rightarrow z_n + \frac{z_c}{2d}. \quad (22)$$

If the energy of a neighbor becomes supercritical through this process, the neighbor in turn *tumbles*. A series of tumbles (an *avalanche*) can result from the dropping of a single grain, ending only when all sites are again just critical or subcritical. The only dissipation comes at the edges of the lattice where grains may “fall off.” If this process is carried on long enough and on a large enough lattice, the system reaches a stationary state where the sizes of avalanches (total number of tumbles resulting from the dropping of one grain) and several other statistical properties of the system obey power law distributions. It was originally suggested that this self-organization was an inherent property of the system, while it now seems established that the system is actually tuned by waiting until avalanches are over before dropping new grains—this is equivalent to allowing non-local interactions [15,16].

For the BTW sandpile, we define  $\rho_c$  as the probability that any site is critical (one more grain added to that site will cause it to tumble). Then, it is easy to construct a mean field branching process, where the probability distribution of the number of nearest-neighbor sites a tumbling site will cause to tumble in the next update is given by

$$p_i = \binom{2d}{i} \rho_c^i (1 - \rho_c)^{n-1}. \quad (23)$$

This leads us to

$$a \simeq 2d, \quad (24)$$

$$m = \sum_i^{2d} i p_i = 1, \quad (25)$$

and a predicted power law distribution for the size of avalanches  $s(n)$ , again obtained from Eqs. (4)-(7). In

higher dimensions ( $d \gtrsim 6$ ), we expect the branching process model to hold exactly and  $s(n) \sim n^{-3/2}$ . This is supported by numerical simulations. However, for lower dimensions, sandpiles will “interfere” with themselves, and a smaller exponent is found. Attempts to calculate the effects of this “final-state” interaction through renormalization have as yet not been completely successful.

So far, we have ignored dissipation and assumed an infinitesimal driving rate (i.e., allowed one avalanche to finish before another grain is dropped). Incorporating dissipation and a finite driving rate into our calculations of  $p_i$  and  $m$  yields

$$m = \left(1 + \frac{h}{\rho_a g(1 - \epsilon)}\right)^{-1} \quad (26)$$

where  $\rho_a$  is the proportion of sites undergoing an avalanche at an update,  $g \simeq 2d$ ,  $\epsilon$  is a dissipation rate (number of grains falling off the edge of the grid per tumbled grain), and  $h$  is a driving rate (probability for each site to have a grain dropped on it during an update). Again, note that  $h$  is proportional to the rate of introduction of new avalanches, while  $\rho_a g(1 - \epsilon)$  is proportional to the rate of growth of existing ones. As in the simpler case where dissipation and driving were ignored, we expect that the branching process model will be quantitatively correct in higher dimensions. Indeed, such a mean field branching process model can be used to predict quantitative values of some sandpile exponents that hold in all dimensions [17]. Unfortunately, it is computationally very expensive to simulate high-dimensional sandpiles. Fig. 8 shows the results of simulating a two-dimensional BTW sandpile with finite driving rates from  $h \rightarrow 0$  to  $h = 10^{-1}$ . As expected, higher driving rates  $h$  lead to lower  $m$  and distributions farther from power law. A derivation of Eq. (26), as well as more discussion of the sandpile data, can be found elsewhere [18]. Other branching process treatments of sandpile models can be found in Ref. [17] and references therein.

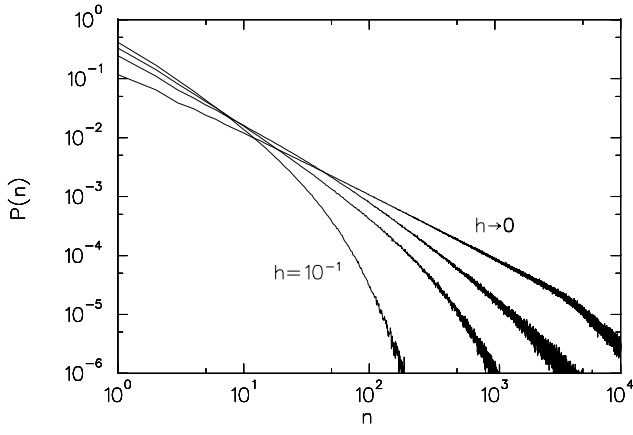


FIG. 8. Avalanche size distribution in the 2-d BTW sandpile model with finite driving rates:  $h = 0, 10^{-3}, 10^{-2}, 10^{-1}$ . Higher driving rates lead to distributions farther from power law and closer to exponential, as predicted by the branching process model. The lattice size for these simulations was  $100 \times 100$  (note the cutoff in the  $h \rightarrow 0$  distribution at  $n \sim 5000$  due to system size effects). Unfortunately, quantitative predictions cannot be made for low-dimensional sandpiles (where “final-state” interactions exist), while simulating high-dimensional sandpiles is computationally prohibitive.

#### IV. DISCUSSION

The Galton-Watson branching process generates power law distributions when its control parameter  $m = 1$ . In all four of the systems we have examined above,

$$m = \left(1 + \frac{R_c}{R_p}\right)^{-1} \quad (27)$$

is determined by the ratio of the rate of introduction of competitors  $R_c$  to the intrinsic rate of growth of existing assemblages  $R_p$ . As this ratio goes to 0,  $m \rightarrow 1$  and the system becomes critical.

This relation can be translated into the standard relation between an *order parameter*

$$\alpha = \frac{R_c}{R_p} \quad (28)$$

and a new form for the control parameter

$$\mu = m^{-1}. \quad (29)$$

Writing  $\alpha$  in terms of  $\mu$ ,

$$\alpha = \begin{cases} (\mu - \mu_c)^\beta & (\mu > \mu_c), \\ 0 & (\mu \leq \mu_c), \end{cases}$$

where  $\mu_c = 1$  and  $\beta = 1$  (Fig. 9). The order parameter represents the rate at which competition is introduced to the system (the strength of selection). A value of the control parameter  $\mu < \mu_c$  implies a system with no competition and no selection—an exponentially growing population. Values of  $\mu$  higher than  $\mu_c$  indicate that new competition is always being introduced and that all existing species or avalanches must eventually die out. When  $\mu = \mu_c$ , competition is introduced at a vanishingly small rate, and we find the critical situation where separation of scales occurs.

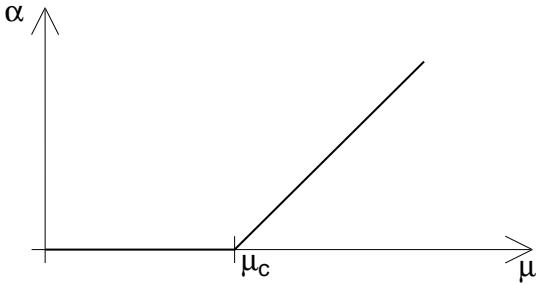


FIG. 9. The order parameter  $\alpha$  as a function of the control parameter  $\mu$ . For  $\mu$  below  $\mu_c$ , the order parameter is 0—organisms (or events) in the system spawn greater and greater number of daughter organisms (events), and there is exponential growth. For  $\mu > \mu_c$ , competition from newly created organisms (events) stops abundances from growing without bound.  $\mu = \mu_c$  marks the critical point where abundances can grow to infinity, but do not show exponential growth, and power law distributions arise.

For sandpile models, this  $\alpha$  is arbitrarily set close to 0 by using large lattice sizes (reducing dissipation) and waiting for avalanches to finish before introducing new perturbations (resulting in an infinitesimal driving rate and a diverging diffusion coefficient). In simulations away from these arbitrary conditions, a loss of criticality is predicted by the model and observed in numerical simulations. Self-organized criticality and its sandpile models have stimulated research in many different fields and systems where near power law avalanche dynamics was observed. It seems that many of these systems should be mappable to branching processes, and that the fractal behavior of these systems and the changes in their dynamics which follow from finite driving rates could be understood in terms of such. For the biological and biologically-inspired systems we have considered, the control parameter is not set arbitrarily at a critical value. However, the dynamics of the evolutionary process, in which it is much harder to effect large jumps in fitness and function than it is to effect small ones, lead to naturally observed values of  $\alpha$  being small, especially for higher taxonomic orders. The dynamics of evolution act, robustly, to keep  $\mu$  near  $\mu_c$ . This in turn leads to a near power law pattern for rank-frequency distributions.

It would be beneficial to compare the predictions of the branching process (BP) model to high-dimensional sandpile simulations, where it should be quantitatively correct. Comparison of the BP model with more biological data is also desirable. For biological systems, there is a vast amount of empirical data, most of it, unfortunately, not in a form suitable for direct comparison to the BP model. Since the model allows a characterization of the abundance distributions with no free parameters, we believe it should be possible to deduct, from abundance distributions (and their divergence from power law), microscopic parameters of the system which created the distribution—e.g., driving rates in sandpiles, genomic and higher-order neutralities in nature. Species abundances are affected by many factors, but we believe that a careful application of the BP model (e.g., by comparison of collections of species with different ecological pressures) could yield insight.

We have shown that the apparent power laws of avalanches in SOC sandpile models, species-abundance distributions in artificial life systems, and rank-abundance distributions in taxonomy can be explained by modelling the dynamics of the underlying system with a simple branching process. This branching process model

successfully predicts, with no free parameters, the observed abundance distributions—including their divergence from power law. This may allow the deduction of the microscopic parameters of the system directly from the macroscopic abundance distribution. We find that we can identify a control parameter—the average number of new events an event directly spawns, and an order parameter—the rate of introduction of competing events into the system, and that these are related in a form familiar from second order phase transitions in statistical physics.

## ACKNOWLEDGMENTS

We would like to thank J. J. Sepkoski for kindly sending us his amended data set for fossil marine animal families. J. C. thanks M. C. Cross for continued support and discussions. Access to the Intel Paragon XP/S was provided by the Center of Advanced Computing Research at the California Institute of Technology. This research was supported in part by NSF Grant No. PHY-9723972.

## APPENDIX A: BINNING METHODS

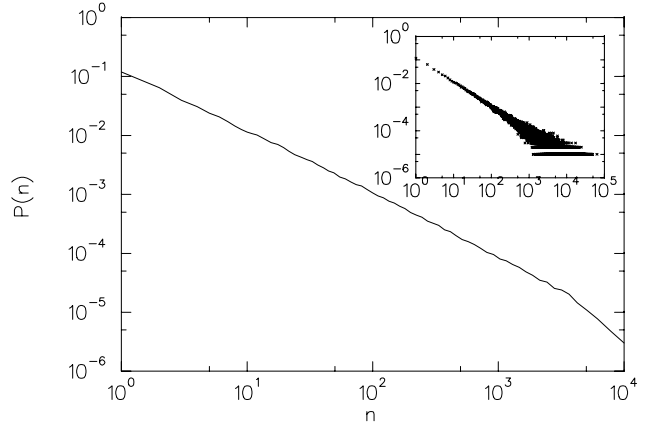


FIG. 10. Binned avalanche size distribution for the BTW sandpile ( $h \rightarrow 0$ ). The inset shows avalanche size distribution data after 100,000 avalanches. The main panel shows the same data binned using the data threshold method with  $T = 1000$ . Overlaying this figure over Fig. 8 (which is the same data for 16 million avalanches) shows no discernible differences between the predictions made by binning and the conclusions given by more data.

When dealing with event distributions best plotted on single log or double log scales (such as exponential and power law distributions), care must be taken in the proper binning of the experimental data. Say we are interested in the probability distribution  $P(n)$  of an event distribution over positive integer values of  $n$ . We conduct  $N$  trials, resulting in a data set  $Q(n)$  of number of events observed for every  $n$  value. For ranges of  $n$  where

the expected or observed number of events for each  $n$  is much higher than 1, normally no binning is required. However, for ranges of  $n$  where  $Q(n)$  or  $P(n)$  is small, binning is necessary to produce both statistically significant data points, and intuitively correct graphical representations. A constant bin size has several drawbacks: One must guess and choose an intermediate bin size to serve across a broad range of parameter space, and the shape and slopes of the curve (even in a double log plot) are distorted [10]. These disadvantages can be overcome by using a variable bin size. However, choosing bin sizes for variable binning is time-consuming and arbitrary—different choices will lead to different conclusions. We propose two related methods of systematically determining appropriate variable bin sizes. Both methods lead to binned data which help in visualizing the underlying distribution (slopes and shapes are conserved).

For the first method (the *Data Threshold Method*), we start by selecting a threshold value  $T$ . Starting from  $n = 1$  and proceeding to higher values, no binning is done until a value of  $n$  is found for which  $Q(n) < T$ . When such a value  $n_s$  is found, subsequent  $Q(n)$  values are added to this amount until the sum of these values is greater than the threshold value,

$$\sum_{n=n_s}^{n_l} Q(n) > T. \quad (\text{A1})$$

We then have a bin size  $(n_l - n_s + 1)$ , with value  $\sum_{n=n_s}^{n_l} Q(n)$ . When plotting, it is convenient to plot this as a single point at the midpoint of  $[n_s, n_l]$ , with an averaged value,

$$\left( \frac{n_s + n_l}{2}, \frac{\sum_{n=n_s}^{n_l} Q(n)}{n_l - n_s + 1} \right). \quad (\text{A2})$$

This yields a graphical representation with little distortion and good predictive power (Fig. 10). This binning procedure is continued until no more data remains to be binned.

The second binning method (the *Template Threshold Method*), uses a predicted probability distribution  $P(n)$ , or a reasonable surrogate. Again, we define a threshold value for fitting  $T$ . However, in this case, the bin sizes are determined by comparing values of the *expected distribution*

$$E(n) = P(n) \times N \quad (\text{A3})$$

to  $T$ . Starting from  $n = 1$  and proceeding to higher values, no binning is done until a value of  $n$  is found for which  $E(n) < T$ . When such a value  $n_s$  is found, subsequent  $E(n)$  values are added to this amount until the sum of these values is greater than the threshold value,

$$\sum_{n=n_s}^{n_l} E(n) > T. \quad (\text{A4})$$

We then have a bin of  $[n_s, n_l]$  with corresponding size  $(n_l - n_s + 1)$ . The average value associated with this bin is

$$\frac{\sum_{n=n_s}^{n_l} Q(n)}{n_l - n_s + 1}. \quad (\text{A5})$$

This procedure is repeated until the data is exhausted. For this method, the data may be graphically represented either as a single point per bin (as in the data threshold method above), or as a point (showing the associated average value) for each measured (non-zero) data point  $Q(n)$ .

The data threshold method requires no *a priori* knowledge, and is a good predictor of the underlying distribution. However, when there are few data points, the template threshold method is more reliable. For both methods, a range of  $T$  should be tried and the best  $T$  (neither over- or under-binning) chosen.

- 
- [1] G. Gutenberg and C. F. Richter, *Ann. Geophys. (C.N.R.S.)* **9**, 1 (1956).
  - [2] M. Stemmler, M. Usher, and Z. Olami, *Phys. Rev. Lett.* **74**, 326 (1995).
  - [3] P. Bak, C. Tang, and K. Wiesenfeld, *Phys. Rev. Lett.* **59**, 381 (1987).
  - [4] B. Burlando, *J. theor. Biol.* **146**, 99 (1990); B. Burlando, *J. theor. Biol.* **163**, 161 (1993).
  - [5] F. Spitzer, *Principles of Random Walk*. (Springer-Verlag, New York, 1964).
  - [6] T. E. Harris, *The Theory of Branching Processes* (Springer, Berlin; Prentice-Hall, Englewood Cliffs, N.J., 1963).
  - [7] H. W. Watson and F. Galton, *J. Anthropol. Inst. Great Britain and Ireland* **4**, 138 (1874).
  - [8] C. Adami, C. T. Brown, and M. R. Haggerty, *Lecture Notes in Artificial Intelligence* **929**, 503 (1995).
  - [9] J. Chu and C. Adami, in *Artificial Life V: Proceedings of the Fifth International Workshop on the Synthesis and Simulation of Living Systems*, edited by C. G. Langton and K. Shimohara, p.462 (MIT Press, Cambridge, 1997).
  - [10] C. Adami, *Introduction to Artificial Life* (Springer, New York, 1998).
  - [11] J. Chu and C. Adami, A simple explanation for taxon abundance patterns. KRL preprint MAP-242 (December 1998).
  - [12] G. U. Yule, *Proc. Roy. Soc. London Ser. B* **213**, 21 (1924).
  - [13] D. M. Raup, *Paleobiology* **11**, 42 (1985).
  - [14] J. J. Sepkoski, *A Compendium of Fossil Marine Animal Families*, 2nd ed. (Milwaukee Public Museum; Milwaukee, WI; 1992) with emendations by J. J. Sepkoski based largely on *The Fossil Record 2*, M. J. Benton, ed. (Chapman & Hall; New York; 1993).
  - [15] D. Sornette, A. Johansen, and I. Dornic, *J. Phys. I* **5**, 325 (1995).

- [16] L. Gil and D. Sornette, Phys. Rev. Lett. **76**, 3991 (1996).
- [17] A. Vespignani and S. Zapperi, Phys. Rev. E **57**, 6345 (1998).
- [18] J. Chu and C. Adami, Non-critical sandpiles. KRL preprint MAP-243 (December 1998)